Pergamon

Chaos, Solitons & Fractals, Vol. 8, No. 4, pp. 499–515, 1997

0960-0779/97 $17.00 + 0.00

PII: S0960-0779(96)00110-5

Hopf Bifurcation in Rotors Supported in Gas Bearings

KRZYSZTOF CZOŁCZYŃSKI and TOMASZ KAPITANIAK

Division of Dynamics, Technical University of Łodz, Stefanowskiego 1/15, 90-924 Łodz, Poland

Abstract—In this paper we describe a problem of control of the Hopf bifurcation. We illustrate the problem by three examples of a rotor system supported in two gas bearings. The bearing bushes are connected to the casing by means of additional air rings. In the case when parameters of the air ring are improperly chosen, at a sufficiently high rotational velocity the rotor undergoes the Hopf bifurcation and the bearing may be damaged by the growing amplitude of self-excited vibrations. We may avoid this danger by a proper selection of stiffness and damping coefficients of the air ring or, in the worst case, by a temporary change of the stiffness or damping coefficients of the air ring. Our method then guarantees a safe passage through the unstable zone between the Hopf and reversed Hopf bifurcation points. © 1997 Elsevier Science Ltd

NOMENCLATURE

B	inertial moment of rotor
B_p	inertial moment of joint bushes
c_1	radial clearance of bearing [m]
c_2	radial clearance of air ring [m]
C_{ij}	damping coefficients of gas film
C_p	damping coefficient of elastic support
F_z	static loading of rotor
K_{ij}	stiffness coefficients of bearing
K_p	stiffness coefficient of elastic support
l	half of the distance between bearings
l_C	half of the distance between dampers
l_K	half of the distance between springs
L	length of bearing and air ring [m]
m	mass of rotor
m_p	mass of joint bushes
p_a	atmospheric pressure [N/m^2]
p_0	supply pressure [N/m^2]
R_1	radius of bearing [m]
R_2	radius of air ring [m]
r_{01}	radius of feedholes of bearing [m]
r_{02}	radius of feedholes of air ring [m]
t	dimensional time [s]
x_c	displacement of journal related to c_1
x_p	displacement of bush related to c_1
Λ	bearing number (dimensionless rotational velocity)
μ	gas viscosity [Ns/m]
τ	time
ω	dimensional rotational velocity [rad/s]

1. INTRODUCTION

The vast majority of the numerous efforts put into the study of dynamical systems in the past 20 years or so have been devoted to long time behaviour of the solutions and to the character of the asymptotic attractors of the system. The tools and techniques of the quantitative description, such as Lyapunov exponents and various invariant measures, have naturally been driven by the need for characterization of these attractors, and relatively little attention has been paid to the transient behaviour of trajectories during their progress from initial conditions to the appropriate attractor. Nevertheless, in a wide range of physical contexts, properly modelled by dynamical systems, the practical interest lies precisely in this behaviour; indeed, the asymptotic attractor may not even be closely approached during the

time interval of interest. In mechanical systems, such as those involving rotating components, it is common for the approach from an initial state to a final, often quite simple, state described by a fixed equilibrium point or limit cycle, to pass through the regions of phase space which are quite unacceptable for the user. Thus, a rotating shaft may develop large oscillations and collide with its bearing whilst slowing down to rest. In such situations the control of (perhaps chaotic) transients is required. A number of methods by which undesirable chaotic behaviour can be controlled or eliminated have been developed [1–10]. More speculatively, they indicate ways in which the existence of chaotic behaviour may be directly beneficial or exploitable. Some of these methods have been successfully applied in engineering systems [1, 2, 5, 7].

Chaos controlling methods, like most of the results in the theory of dynamical systems, have an asymptotic character [11–13], i.e. under given conditions a dynamical system with specified parameters behaves in a particular way when $t \to \infty$. Because many real systems, like the rotor system mentioned above, are characterized by some values of parameters only for finite time, these controlling methods cannot always be practically implemented and there is a need to develop efficient methods for control of transient non-linear effects.

In this paper we investigate the problem of practical control of the Hopf bifurcation. We consider a particular but representative example of such a situation. For $a = a_w$, which is a desired working condition, let the dynamical system

$$\dot{x} = f(a,x), \tag{1}$$

where $x \in \mathbb{R}^n$, $a \in \mathbb{R}^m$ ($n, m = 1,2,\ldots$) is a vector of system parameters, be characterized by steady-state behaviour (i.e. $x = 0$ is a stable fixed point for $a = a_w$). Suppose further that to reach practically the value $a = a_w$ from $a = a_s$ (the starting point), a has to go through the interval $[a_1,a_2]$, and then, for $a \in [a_1,a_2]$, the steady state $x = 0$ of the dynamical system (1) is unstable as the system undergoes the Hopf bifurcation at $a = a_1$ and reversed Hopf bifurcation at $a = a_2$. We try to answer the following question: can we safely reach the desired working condition $a = a_w$ or do we have to restrict ourselves to the parameter range $a < a_1$?

2. CONTROLLING PROCEDURE

The situation described is characteristic for rotor systems where the rotor rotational velocity Λ is a system parameter which has to increase continuously from its starting value $\Lambda = 0$ to $\Lambda = \Lambda_w$ (desired working conditions), when in the interval $[\Lambda_1,\Lambda_2]$, where $\Lambda_{1,2} < \Lambda_w$, the steady state $x = 0$ is unstable. A passage through this interval, as exemplified in Fig. 1, is associated with an increase in the amplitude of rotor vibrations as at Λ_1 the self-excited vibrations originate and are added to small oscillations due to unbalance. At the value Λ_2 the self-excited vibrations decrease, and the amplitude of vibrations stabilizes at the final value. In the majority of practical systems the interval (Λ_1, Λ_2) cannot be passed safely, and the self-excited oscillations can damage the system at $\Lambda = \Lambda_d$ (Fig. 2) as the acceptable increase in the vibration amplitude is limited by the design restrictions.

The easiest way to avoid the danger of the system damage is to design it in a way which completely eliminates the Hopf bifurcation from the system operation in the whole range (Λ_s, Λ_w). As follows from our numerical investigations concerning rigid rotors supported in

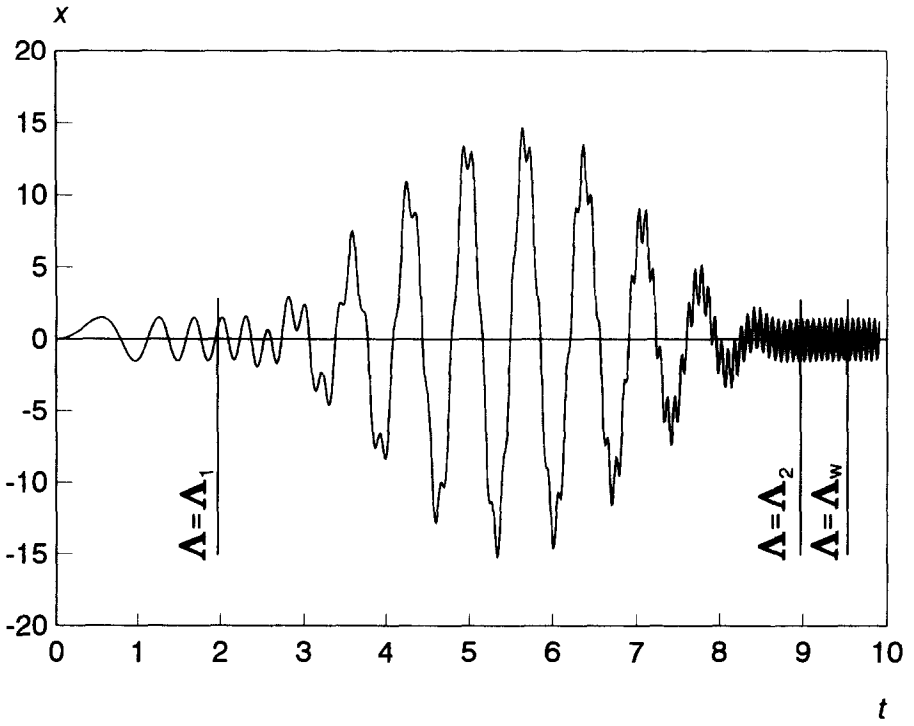

Fig. 1. Unbalanced and self-excited vibrations of a mechanical system.

gas journal bearings, in some cases it is not possible to design the system in such a way. Then, the transient behaviour in the dangerous zone has to be controlled so that it may be passed safely. In this case we propose a simple method which is based on a small temporary change of one of the other components of the vector a of system parameters, which allows us to stabilize the fixed point $x = 0$. When the dangerous zone is passed, the vector a returns to its initial value. In the controlled system the passage through the dangerous zone is shown in Fig. 3.

3. OBJECT OF CONSIDERATIONS: ROTOR SUPPORTED IN GAS BEARINGS WITH ELASTICALLY MOUNTED BUSHES

Let us consider a system (Fig. 4) which consists of a symmetrical rigid rotor supported in two gas bearings. The combined base of both the bearing bushes is connected to the casing by means of linear springs K_p and viscous dampers C_p. The force $2F_z$ is an external static load acting on the rotor, so F_z is the static response of the bearing to the force $2F_z$. The full dynamics of the system was considered in Refs [14–18]. Here we describe only one particular case as the illustration of our method of elimination of self-excited vibrations from the system operation.

As follows from the references mentioned above, the elastic support K_p, C_p of the bearing bushes makes it possible to avoid self-excited vibrations when values of these coefficients are properly chosen. The main problem is how to design such an elastic support. Our

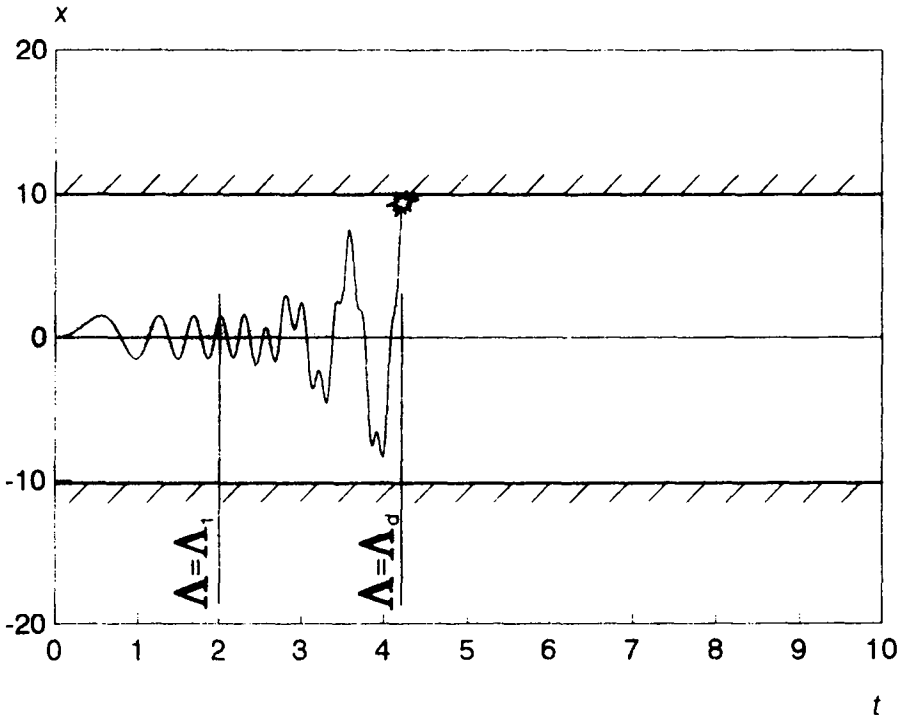

Fig. 2. Unbalanced and self-excited vibrations of a mechanical system with limited amplitude of vibrations.

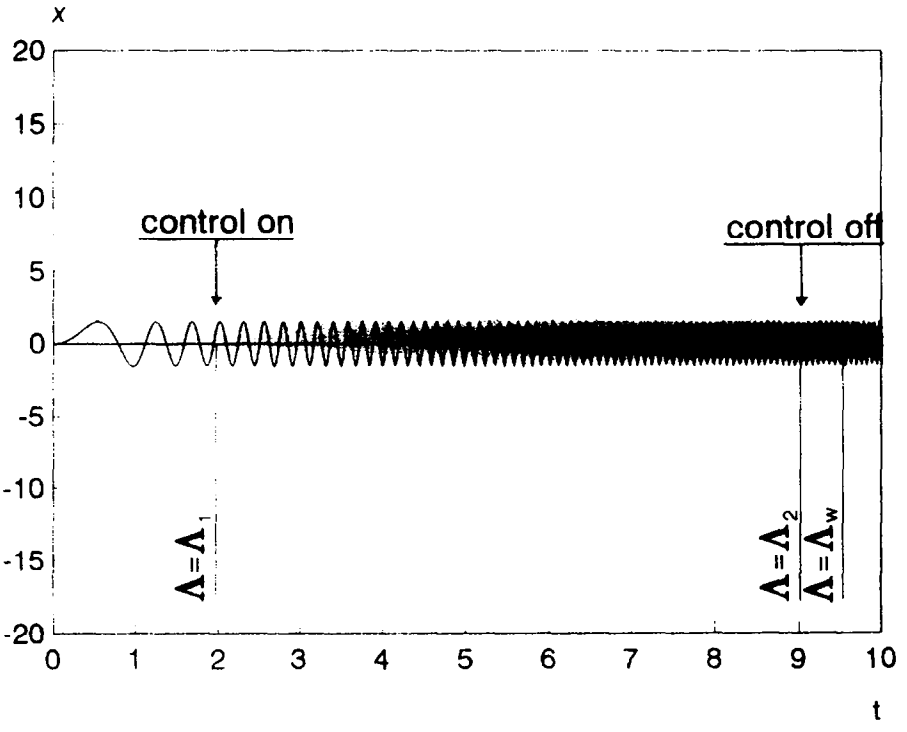

Fig. 3. Vibrations of a mechanical system with Hopf bifurcation control.

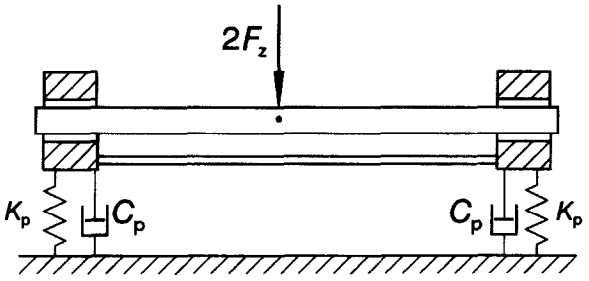

Fig. 4. Rotor supported in gas bearings with bushes mounted in springs and dampers.

proposition is to introduce an additional air ring **6** (Fig. 5) round each of the bearing bushes **3**. As the bushes do not rotate, these rings must of course be externally pressurized. As follows from our previous considerations, the chamber feeding system must be employed, in which the air goes from the compressor through the orifices r_{d1} (or r_{d2}) into chambers **1**, and then through the feedholes r_{02} into the gap of the air ring. The dependence between the displacements x_p, y_p of the bush from the static equilibrium position and the resulting dynamic increments in the force are given as

$$\begin{Bmatrix} \delta F_{zx} \\ \delta F_{zy} \end{Bmatrix} = \begin{bmatrix} C_{11} & C_{12} \\ C_{21} & C_{22} \end{bmatrix} \begin{Bmatrix} \dot{x} \\ \dot{y} \end{Bmatrix} + \begin{bmatrix} K_{11} & K_{12} \\ K_{21} & K_{22} \end{bmatrix} \begin{Bmatrix} x \\ y \end{Bmatrix} \tag{2}$$

while in the supporting system from Fig. 4 they are

$$\begin{Bmatrix} \delta F_{zx} \\ \delta F_{zy} \end{Bmatrix} = \begin{bmatrix} C_p & 0 \\ 0 & C_p \end{bmatrix} \begin{Bmatrix} \dot{x} \\ \dot{y} \end{Bmatrix} + \begin{bmatrix} K_p & 0 \\ 0 & K_p \end{bmatrix} \begin{Bmatrix} x \\ y \end{Bmatrix}. \tag{3}$$

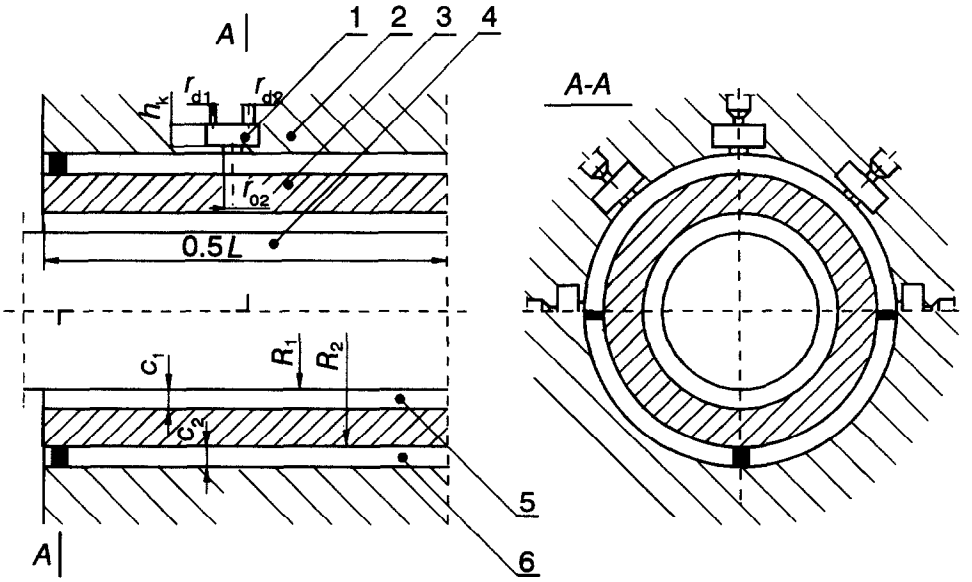

Fig. 5. Air ring: a design of an elastic support of a bearing bush (1: chamber, 2: casing, 3: bush, 4: rotor, 5: bearing gap, 6: air ring).

As the bush does not rotate, the cross-coupling coefficients C_{12}, C_{21}, K_{12}, K_{21} are negligibly small and, as the bush-casing eccentricity ratio is less than 0.25, the main coefficients $C_{11} \approx C_{22}$ and $K_{11} \approx K_{22}$. We may also assume that (approximately) for the air ring the following equation is satisfied:

$$\begin{Bmatrix} \delta F_x \\ \delta F_y \end{Bmatrix} \approx \begin{bmatrix} C_{11} & 0 \\ 0 & C_{22} \end{bmatrix} \begin{Bmatrix} \dot{x} \\ \dot{y} \end{Bmatrix} + \begin{bmatrix} K_{11} & 0 \\ 0 & K_{22} \end{bmatrix} \begin{Bmatrix} x \\ y \end{Bmatrix},$$

which is similar to eqn (3). This assumption allows us to predict, from calculations concerning the system with linear springs K_p and viscous dampers C_p, what values of the stiffness and damping coefficients of the designed air ring will ensure the steady-state stability.

The data of the air ring considered are as follows: length $L = 0.11$ m, radius $R_2 = 0.065$ m, radial clearance $c_2 = 30 \times 10^{-6}$ m, air viscosity $\mu = 18.2 \times 10^{-6}$ kg m^{-1} s^{-1}. The feeding system consists of 16 feedholes, located in two rows at 1/4 and 3/4 of the length of the ring, supply pressure $p_0 = 0.7 \times 10^6$ Pa, radius of the orifices $r_d = 0.15 \times 10^{-3}$ m or 1.0×10^{-3} m, radius of the feedholes $r_{02} = 1.0 \times 10^{-3}$ m.

Two parameters of the feeding system decide about values of the main stiffness and damping coefficient of the air ring: the volume of the chambers and the radius of the orifices. The volume of the chamber $V = \pi r^2 h_k$ is proportional to the height h_k as the radius $r = 5.0 \times 10^{-3}$ m is constant. Figure 6 shows the values of C_{11} and K_{11} as functions of the frequency of vibrations ν for three different values of the chamber height $h_k = 0.03$, 1.0 and 9.0×10^{-3} m. As can be seen, for small values of $h_k = 0.03$ m, the damping coefficient is positive but very small and the stiffness coefficient is relatively big ($K_{11} \approx 17$). An increase of the volume of the air chambers at first causes the 'air hammer' phenomenon ($C_{11} < 0$) to appear for small values of ν. Furthermore, the C_{11} values increase and the 'air hammer' area shifts below the natural frequency range of the investigated rotor. Concurrently, one can

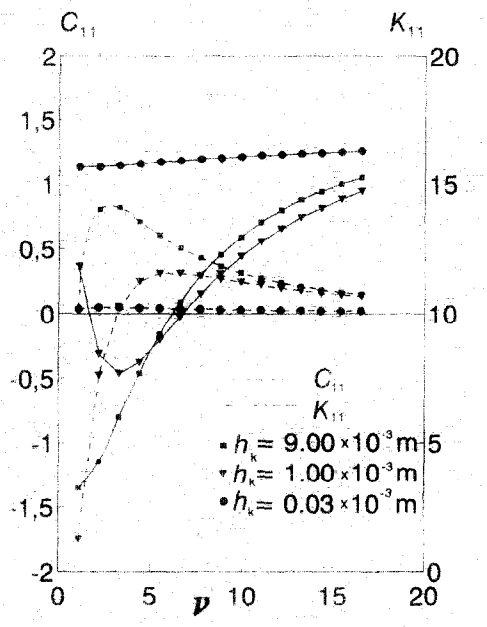

Fig. 6. Stiffness and damping coefficients of air ring ($r_d = 0.15 \times 10^{-3}$ m).

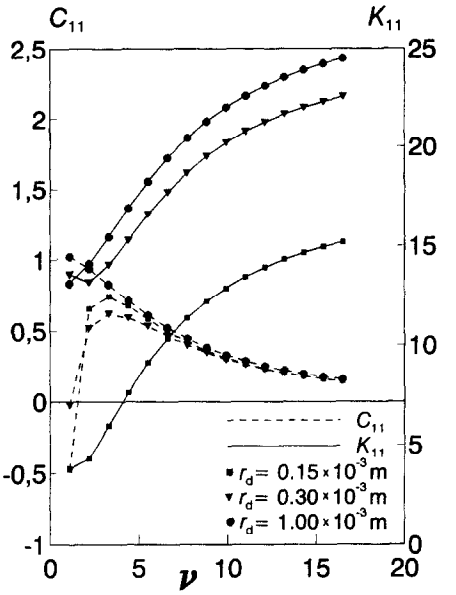

Fig. 7. Stiffness and damping coefficients of air ring ($h_k = 6.0 \times 10^{-3}$ m).

observe a significant decrease of the stiffness coefficient value K_{11}. Figure 7 shows how the radius of the orifice r_d influences the stiffness and damping coefficients. Enlargement of r_d causes an increase of the K_{11} coefficient. In the region of higher frequencies one cannot observe any influence of the radius of the orifice on the damping coefficient values. In the neighbourhood of the 'air hammer' region when the r_d value decreases, one can observe the sudden diminishing of C_{11} and the 'pneumatic resonance' phenomenon. It is intelligible because, when the radius of the orifice increases, the pressure in the chamber is closer and closer to the supply pressure p_0, which means that the chamber feeding system operates in the same way as the direct action feeding system. One cannot observe the 'pneumatic hammer' phenomenon in the direct feeding systems.

4. EXAMPLE I

In our first example we consider the rotor whose data are: mass $m = 0.42$, moment of inertia $B = 42$, distance between the bearings $2l = 34.6$. The parameters of the bushes (combined by a common base) are: mass $m_p = 0.12$, moment of inertia $B_p = 36$, distance between the springs and dampers $2l_K = 2l_C = 2l$. The rotor is supported in the externally pressurized bearings whose data are: length $L = 0.11$ m, radius $R_1 = 0.055$ m, radial clearance $c_1 = 30 \times 10^{-6}$ m. The feeding system of the bearings consists of 16 feedholes (radius $r_{01} = 1.0 \times 10^{-3}$ m), located in two rows at 1/4 and 3/4 of the length of the bearing, supply pressure $p_0 = 0.7 \times 10^6$ Pa. The rotor is loaded by its weight $2F_z = 7$.

Figures 8 and 9 show the stability maps of the system for three selected values of the stiffness coefficient $K_p = 4$, 8 and 16, and for various values of the damping coefficient C_p. Figure 8 shows the regions (hatched) where the self-excited vibration of cylindrical modes appear, and Fig. 9 presents the regions of the self-excited vibrations of conical modes.

When the bearing bushes are supported in the air rings with $r_d = 0.15 \times 10^{-3}$ m and $h_k = 0.03 \times 10^{-3}$ m, the stiffness coefficient $K_{11} \approx 16$ and the damping coefficient $C_{11} \approx 0.06$

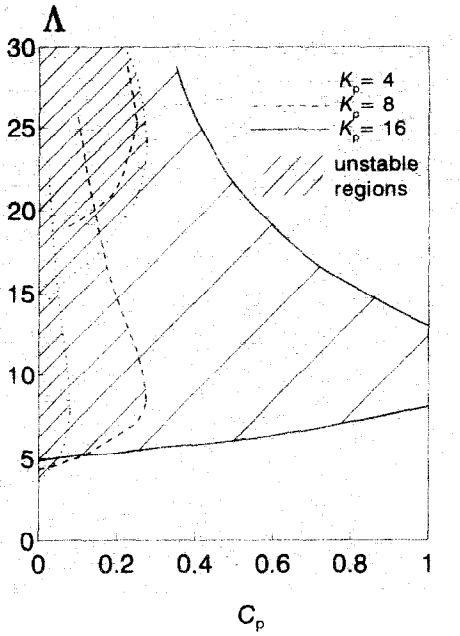

Fig. 8. Stability map of rotor supported in gas bearings with bushes mounted in springs and dampers: vibrations with cylindrical modes.

(see Fig. 6). As we can see from Figs 8 and 9, for these values of K_p and C_p at the rotational velocity $\Lambda \approx 5$, the self-excited vibrations with cylindrical modes appear. This fact is confirmed by Fig. 10(a), which shows the real (η_i) and imaginary (ν_i) parts of four basic

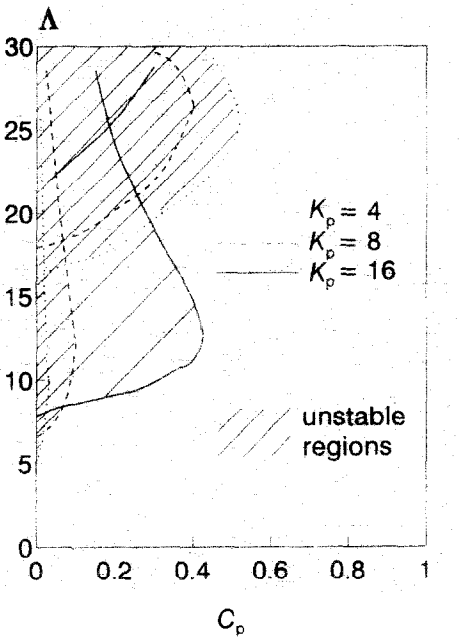

Fig. 9. Stability map of rotor supported in gas bearings with bushes mounted in springs and dampers: vibrations with conical modes.

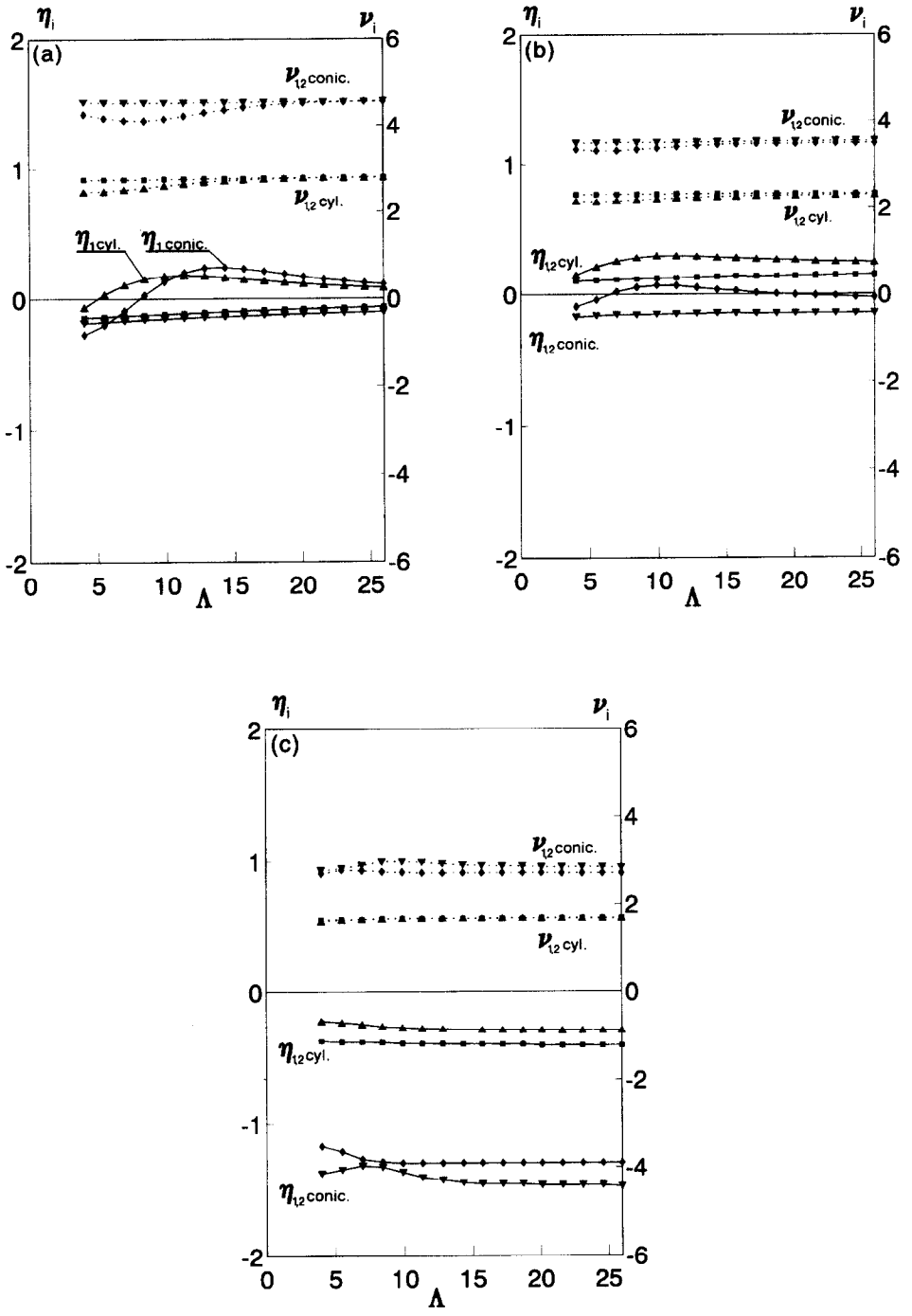

Fig. 10. Eigenvalues $\lambda_i = \eta_i + j\nu_i$ of rotor with bushes supported in air ring, $r_d = 0.15 \times 10^{-3}$ m: (a) $h_k = 0.03 \times 10^{-3}$ m, (b) $h_k = 1.0 \times 10^{-3}$ m, (c) $h_k = 9.0 \times 10^{-3}$ m.

eigenvalues of the system in which the springs K_p and the dampers C_p are replaced by the described air ring: at $\Lambda \approx 5$ the real part η_{1cyl} changes from negative to positive, i.e. the steady state becomes unstable. Additionally, if it were possible to increase Λ over $\Lambda = 5$

(without damage to the bearings), at $\Lambda \approx 8$, vibrations with conical modes would become unstable ($\eta_{1\text{conic}}$ becomes positive).

When we increase the volume of the chambers ($h_k = 1.0 \times 10^{-3}$ m), the basic free cylindrical and conical vibrations of the system are in the range $2 < \nu < 3.5$. This means (Fig. 6) that the stiffness coefficient $K_{11} \approx 8$ and (which is most important) the damping coefficient C_{11} is negative. The system undergoes the 'pneumatic hammer' phenomenon and, as can be seen from Fig. 10(b), the real parts η_{1cyl}, η_{2cyl} of vibrations with cylindrical modes are positive in the whole range of Λ.

The air ring is designed properly when $h_k = 9.0 \times 10^{-3}$ m. For this case, the basic free cylindrical and conical vibrations of the system are in the range $1.7 < \nu < 3$, so (see Fig. 6) the stiffness coefficient $K_{11} \approx 4$ and the damping coefficient $C_{11} \approx 0.8$. For $K_p = 4$ and $C_p = 0.8$, no unstable regions can be observed in Figs 8 and 9. This fact is confirmed in Fig. 10(c), all the real parts of four basic eigenvalues are negative. We have eliminated self-excited vibrations from the system operation.

5. EXAMPLE II

As our second example, we show the stability problem of the rotor whose parameters are as follows: mass $m = 0.42$, moment of inertia $B = 126$, distance between the bearings $2l = 34.6$. The parameters of the bushes (combined by a common base) are: mass $m_p = 0.12$, moment of inertia $B_p = 36$, distance between the springs and dampers $2l_K = 2l_C = 2l$. The parameters of the bearings are: length $L = 0.11$ m, radius $R_1 = 0.055$ m, radial clearance $c = 30 \times 10^{-6}$ m, but this time the bearings are self-acting. As in Example I, the rotor is loaded by the weight $2F_c = 7$.

Figure 11 shows a stability map of the system for two selected values of the stiffness coefficient $K_p = 5$ and 16, and for various values of the damping coefficient C_p. In this example, parameters of the rotor have been selected in such a way that the system has the same eigenvalues as cylindrical and conical modes. As we can see from Fig. 11, when the stiffness coefficient $K_p = 16$, a wide unstable region exists for any value of the damping coefficient C_p. If we support the bearing bushes in the air rings with $h_k = 6.0 \times 10^{-3}$ m and $r_d = 1.0 \times 10^{-3}$ m ($r_d = r_{02}$, which means that the air ring has an almost direct feeding system), then the main stiffness coefficient of the ring $K_{11} = 16$, and the damping coefficient $C_{11} = 0.9$ (Fig. 7 for $\nu = 2.7$). As follows from Fig. 11, for $K_p = 16$ and $C_p = 0.9$ at $\Lambda = 5$, the system should undergo the Hopf bifurcation, and at $\Lambda = 14$ the reversed Hopf bifurcation. Figure 12(a) shows that the real part η_1 of the lowest eigenvalue indeed becomes positive at $\Lambda = 5$ and then back negative at $\Lambda = 15$.

We may eliminate self-excited vibrations by changing the radius of the orifice (not the volume of the chambers, as in Example I) from $r_d = 1.0 \times 10^{-3}$ m to $r_d = 0.15 \times 10^{-3}$ m. After this change, K_{11} diminishes from 16 to 5, and C_{11} from 0.9 to 0.75 (Fig. 7 for $\nu = 1.7$). For such values of K_p and C_p, there are no unstable regions in Fig. 11. We may observe a confirmation of the elimination of the Hopf bifurcation in Fig. 12(b); in the whole range of the rotational velocity Λ, both real parts of the eigenvalues are negative.

Figure 13 shows amplitudes of vibrations of the journal (x_c-solid lines) and of the bush (x_p-broken lines) in the plane in which the force F_c acts, as functions of the rotational velocity Λ. As can be seen, when $r_d = 1.0 \times 10^{-3}$ m [Fig. 13(a)], in the range $7.5 < \Lambda < 12$ the amplitude of self-excited vibrations of the journal exceeds the value which is permitted by the radial clearance of the bearing and the value of the journal: bush eccentricity ratio.

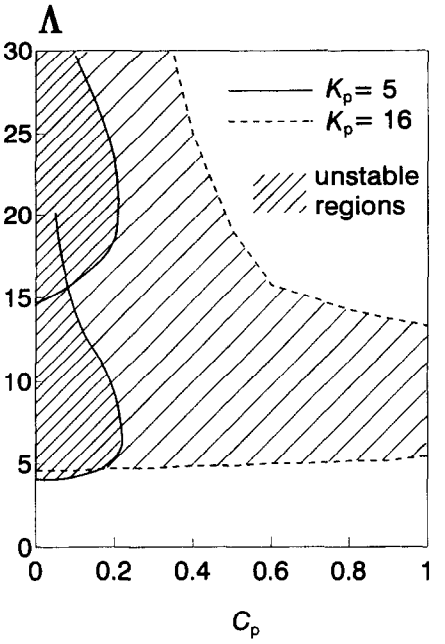

Fig. 11. Stability map of rotor supported in gas bearings with bushes mounted in springs and dampers: vibrations with cylindrical modes = vibrations with conical modes.

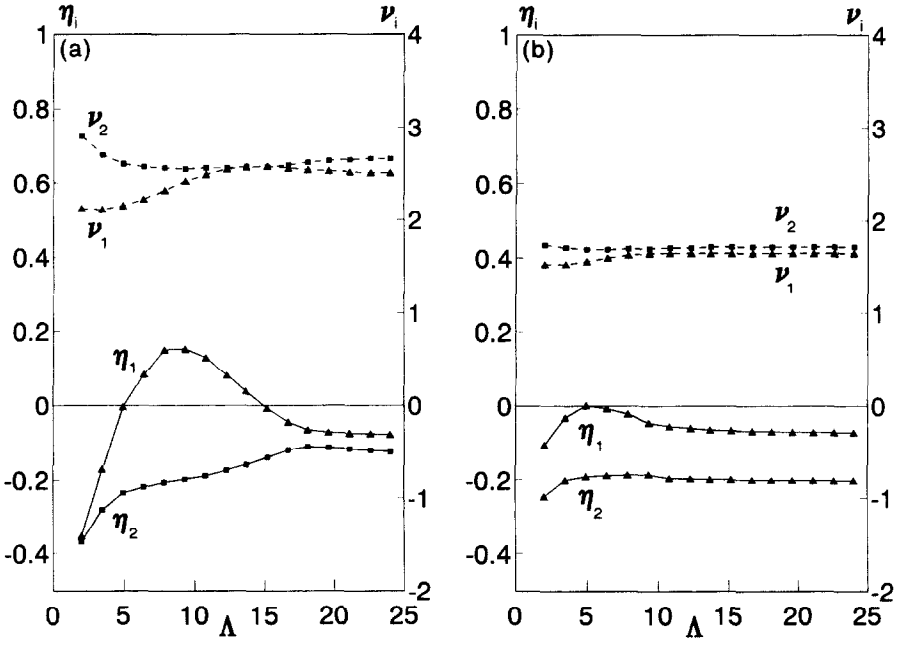

Fig. 12. Eigenvalues $\lambda_i = \eta_i + j\nu_i$ of rotor with bushes supported in air ring, $r_{02} = 1.0 \times 10^{-3}$ m, $h_k = 6.0 \times 10^{-3}$ m: (a) $r_d = 1.0 \times 10^{-3}$ m, (b) $r_d = 0.15 \times 10^{-3}$ m.

When $r_d = 0.15 \times 10^{-3}$ m [Fig. 12(b)], only the unbalanced vibrations and the small resonance of the bush but no self-excited vibrations can be observed.

Figure 14 shows the dynamic behaviour of the system in the transient period, after the step change of the loading force from 7 to 12, at the velocity $\Lambda = 21$ over the unstable region for $r_d = 1.0 \times 10^{-3}$ m. As we can see, when $r_d = 1.0 \times 10^{-3}$ m, the free vibrations forced by the step change of the load diminish significantly more slowly than in the case of $r_d = 0.15 \times 10^{-3}$ m; this is an additional advantage of the use of the air ring with a smaller radius of the orifices.

6. EXAMPLE III

In our third example we will consider the stability problem of the system in which the parameters of the rotor and the bushes are the same as in Example II. The parameters of the bearings are also the same as in Example II: length $L = 0.11$ m, radius $R_1 = 0.055$ m, radial clearance $c_1 = 30 \times 10^{-6}$ m, but this time the bearings are externally pressurized. As in Examples I and II, the rotor is loaded by the weight $2F_z = 7$.

Figure 15 shows the stability map of the system for two selected values of the stiffness coefficient K_p and various values of the damping coefficient C_p. Here Λ_w is the assumed working velocity of the rotor. As can be seen, for $K_p = 10$, the system is unstable at the desired working velocity. On the other hand, for $K_p = 20$, the system is stable at Λ_w, but it cannot reach this velocity due to the unstable region below Λ_w. We have solved this problem by changing the stiffness coefficient K_p from $K_p = 20$ to $K_p = 10$ at $\Lambda = \Lambda_1 = 10$, and then again from $K_p = 10$ to $K_p = 20$ at $\Lambda = \Lambda_2 = 25$. The damping coefficient C_p of the elastic support is still equal to 0.5.

The elastic support of the bearing bushes, which allows us to change the stiffness

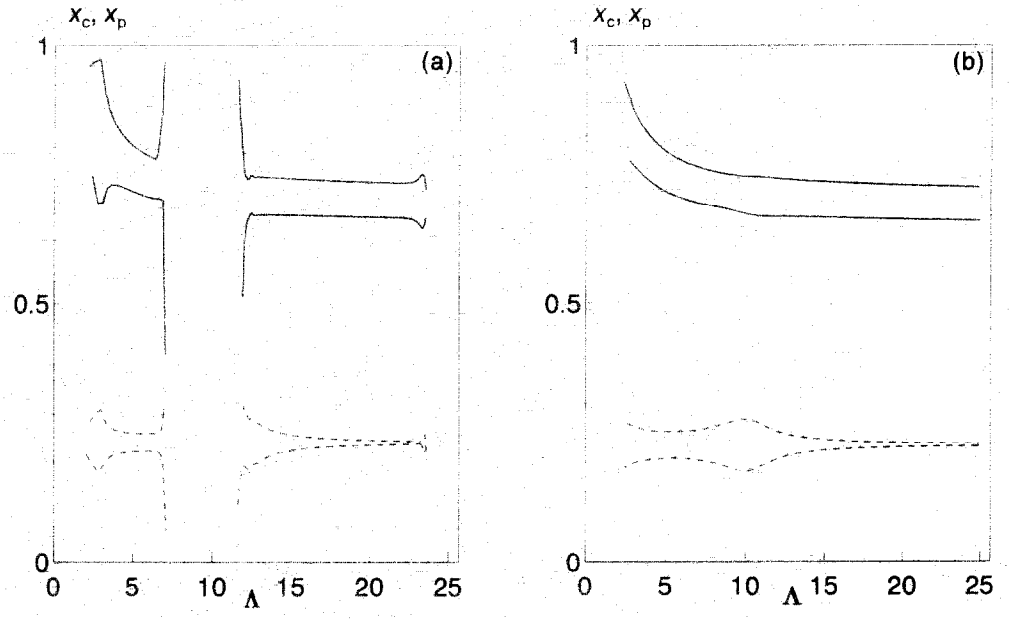

Fig. 13. Amplitudes of unbalanced and self-excited vibrations of rotor (solid lines) and bush (broken lines) in the plane in which the force F_z acts, as functions of the rotational velocity Λ: (a) $r_d = 1.0 \times 10^{-3}$ m, (b) $r_d = 0.15 \times 10^{-3}$ m

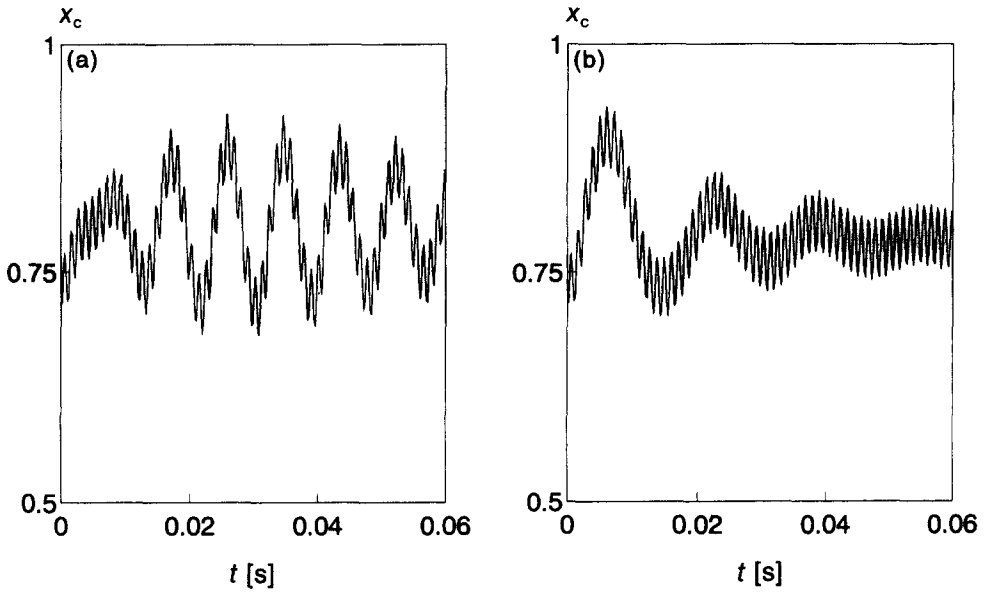

Fig. 14. Dynamic behaviour of the rotor after the step change of the loading force, $\Lambda = 21$: (a) $r_d = 1.0 \times 10^{-3}$ m, (b) $r_d = 0.15 \times 10^{-3}$ m.

coefficient K_p, may be designed as the air ring which is fed by air through one of two orifices with the radius $r_{d1} = 0.15 \times 10^{-3}$m, or $r_{d2} = 1.0 \times 10^{-3}$m.

Figure 16 shows the real (η_i) and imaginary (ν_i) parts of the basic (which may undergo self-excitation) eigenvalues of the system with an air ring. In Fig. 16(a) ($r_d = r_{d1}$), we can see that at $\Lambda \approx 29$, the real part η_2 becomes positive, so the steady state of the system is unstable at the working condition Λ_w. In Fig. 16(b) ($r_d = r_{d2}$), the real part η_1 is positive in the range

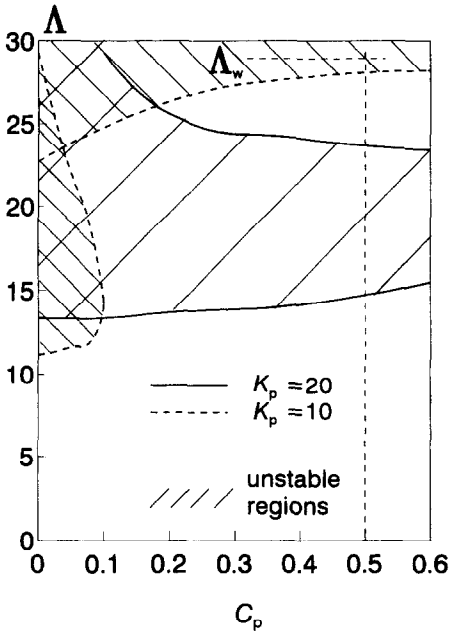

Fig. 15. Stability map of rotor supported in gas bearings with bushes mounted in springs and dampers.

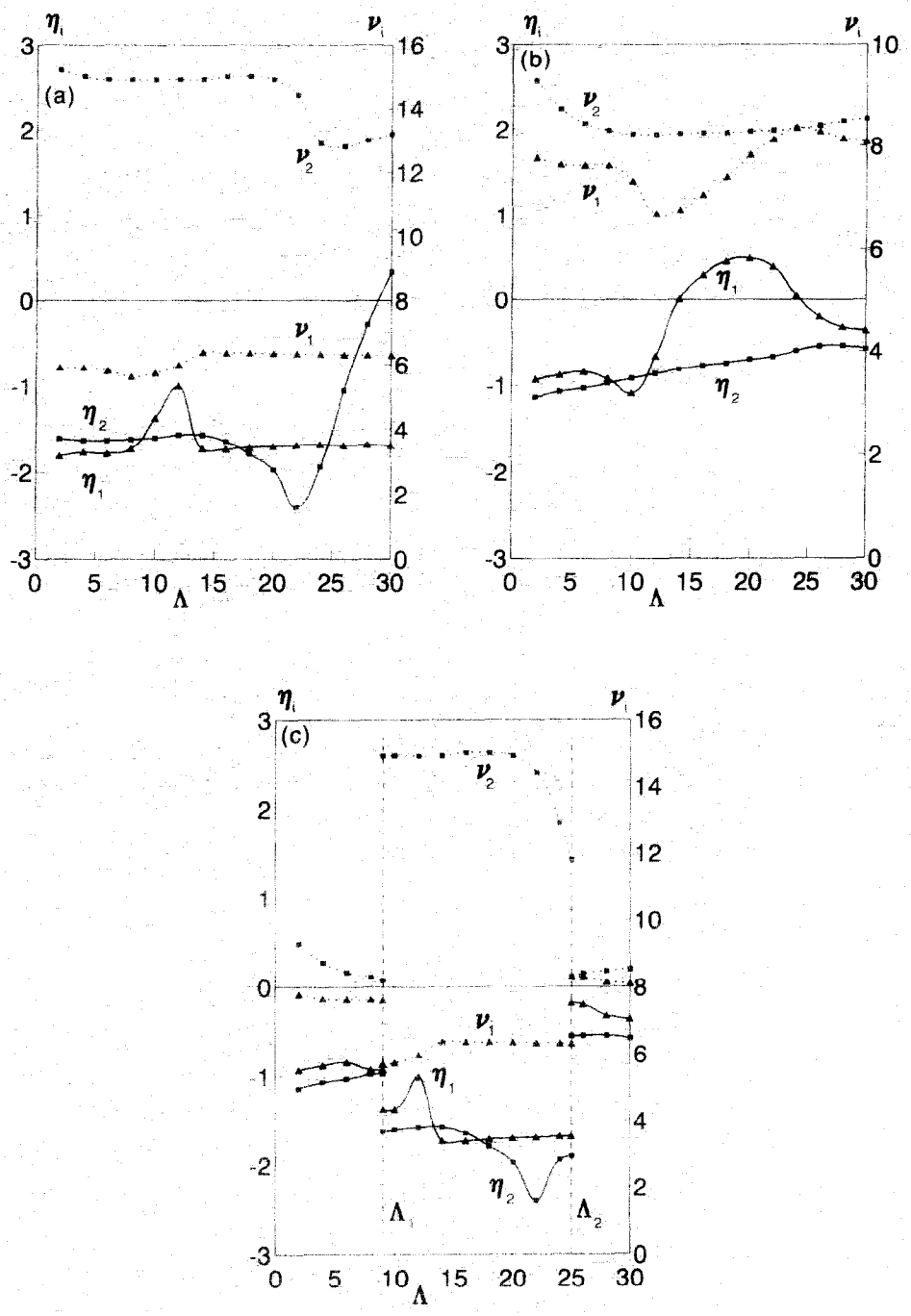

Fig. 16. Eigenvalues $\lambda_i = \eta_i + j\nu_i$ of rotor with bushes supported in air ring. $r_{02} = 1.0 \times 10^{-3}$ m, $h_k = 6.0 \times 10^{-3}$ m: (a) $r_{d1} = 0.15 \times 10^{-3}$ m, (b) $r_{d1} = 1.0 \times 10^{-3}$ m, (c) with control.

$14 < \Lambda < 23$, which corresponds to the hatched unstable region for $K_p = 20$ in Fig. 15. If we temporarily change the radius of the orifices from r_{d2} to r_{d1} at Λ_1, [Fig. 16(c)], and then again from r_{d1} to r_{d2} at Λ_2, we can keep both η_1 and η_2 below zero in the whole range of the rotational velocity Λ.

Figure 17 shows the values of the main stiffness and damping coefficients of the air ring in

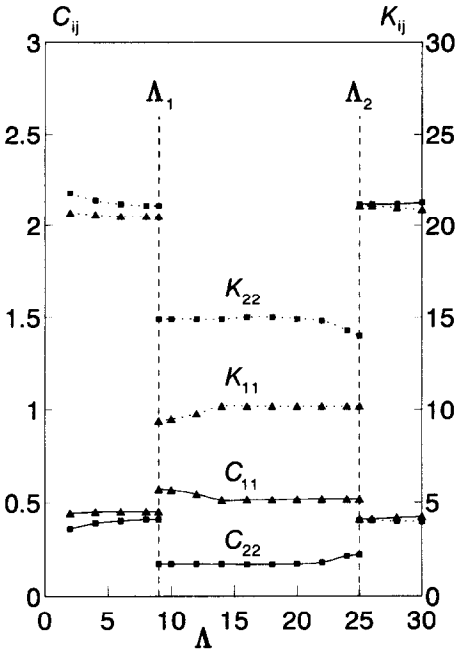

Fig. 17. Stiffness and damping coefficients of the air ring for the system with control.

the system with control. Changes of r_d cause changes in the coefficients. As can be seen, the damping coefficients C_{11} and C_{22} of the air ring may be approximately treated as $C_p \approx 0.5$, and the stiffness coefficients K_{11} and K_{22} are approximately equal to $K_p \approx 10$ for $r_{d1} = 0.15 \times 10^{-3}$m, or $K_p = 20$ for $r_{d2} = 1.0 \times 10^{-3}$m, as is shown on the stability map in Fig. 15.

Figure 18(a) shows the dimensionless amplitudes of the vibrations of the rotor (solid lines) and the bushes (broken lines) in the plane in which the force F_z acts, as functions of the rotational velocity Λ. The radius of the orifices is r_{d1}. In this case, according to Fig. 15, in the wide range $\Lambda < 28$, only small unbalanced vibrations appear. Unfortunately, at $\Lambda = 28$ the system undergoes the Hopf bifurcation and the self-excited vibrations grow rapidly until the working velocity is reached. At $\Lambda = \Lambda_w$ the steady state of the rotor is unstable. Unlike this case, for r_{d2}, the steady state is stable at $\Lambda = \Lambda_w$ [see Fig. 18(b)], but below this velocity, at $\Lambda \approx 14$, the rotor undergoes the Hopf bifurcation (and the reversed Hopf bifurcation at $\Lambda \approx 23$). The passage through the wide unstable zone $14 < \Lambda < 23$ is not possible without a strongly damaging contact between the journals, bushes and casing. In the system with control, with the double chambers in the air ring feeding system, we use the orifices r_{d1} for small values of Λ, then switch the feeding from r_{d1} to r_{d2} at $\Lambda_1 = 10$ ['control on', see Fig. 18(c)], before the self-excited vibrations appear, go through the dangerous zone, and finally switch again ('control off') to r_{d1} at $\Lambda = 25$, reaching safely the working velocity Λ_w. As can be seen, in this case only small unbalanced vibrations of the system are observed. There are no self-excited vibrations again.

7. CONCLUSIONS

We have introduced a method which allows us to control the Hopf bifurcation in transients. Our method guarantees elimination of the self-excited vibrations, or a passage

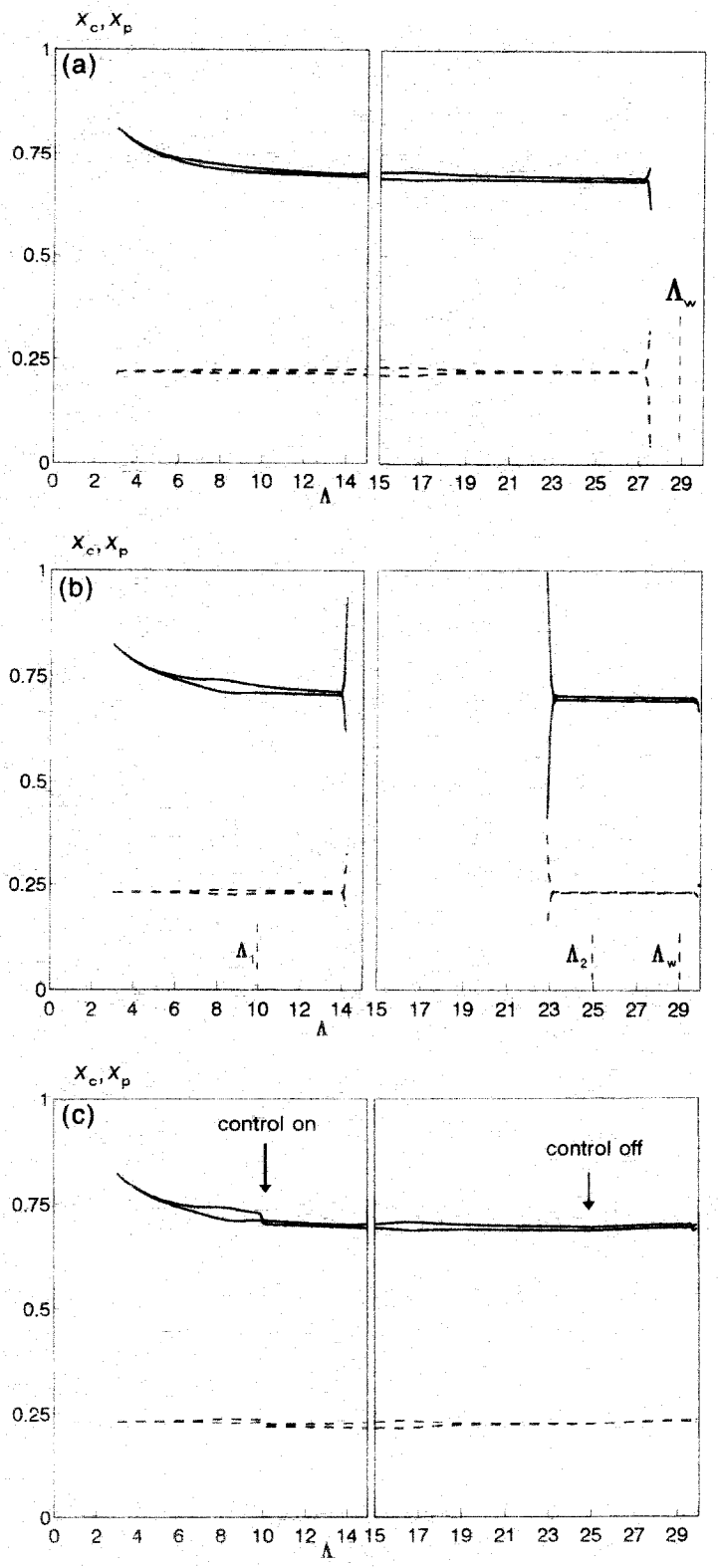

Fig. 18. Amplitudes of vibrations of rotor (solid lines) and bushes (broken lines) in the plane in which the force F_c acts, as functions of the rotational velocity Λ: (a) $r_{c1} = 0.15 \times 10^{-3}$ m, (b) $r_{c1} = 1.0 \times 10^{-3}$ m, (c) system with control.

through the unstable zone between the Hopf and the reversed Hopf bifurcation points. This passage is made possible by a temporary change of one of the system parameters.

Our method can have significant practical applications as it permits an increase in the rotational velocity of rotors in many machines (which is no longer restricted to lower values $\Lambda < \Lambda_1$). In many current engineering systems a small temporary change of one of the system parameters can easily be made, and the method can stimulate the idea of 'non-linear design', i.e. the system can be designed in such a way as to exploit non-linear effects. We hope that the examples considered in this paper will stimulate further research on the transient behaviour of similar non-linear systems.

REFERENCES

1. Blazejczyk, B., Kapitaniak, T., Wojcwoda, J. and Brindley, J., Controlling chaos in mechanical systems. *Appl. Mech. Rev.*, 1993, **46,** 385–391.
2. Dedieu, H. and Ogorzalek, M., Controlling chaos in Chua's circuit via sampled inputs. *Int. J. Bifurc. Chaos*, 1994, **4,** 447–456.
3. Ditto, W. L., Rauseo, S. W. and Spano, M. L., Experimental control of chaos. *Phys. Rev. Lett.*, 1991, **65,** 3211.
4. Dressler, U. and Nitsche, G., Controlling chaos using time delay coordinates. *Phys. Rev. Lett.*, 1992, **68,** 1.
5. Kapitaniak, T., Kocarev, L. and Chua, L. O., Controlling chaos without feedback and control signals. *Int. J. Bifurc. Chaos*, 1993, **3,** 459–468.
6. Ott, E., Grebogi, C. and Yorke, Y. A., Controlling chaos. *Phys. Rev. Lett.*, 1990, **64,** 1196.
7. Pyragas, K., Continuous control of chaos by self-controlling feedback. *Phys. Lett.*, 1992, **170A,** 421.
8. Romeiras, F., Ott, E., Grebogi, C. and Dayawansa, W. P., Controlling chaotic dynamical systems. *Phys. D*, 1992, **58,** 165.
9. Shinbrot, T., Ott, E., Grebogi, C. and Yorke, Y. A., Using chaos to direct trajectories to targets. *Phys. Rev. Lett.*, 1990, **65,** 3215.
10. Tel, T., Controlling transient chaos. *J. Phys. A*, 1991, **24,** L1359.
11. Kapitaniak, T., *Chaotic Oscillations in Mechanical Systems*. Manchester University Press, Manchester, 1991.
12. Moon, F. C., *Chaotic Vibrations*. Wiley, Chichester, 1987.
13. Thompson, J. M. T. and Steward, B., *Nonlinear Dynamics*. Wiley, Chichester, 1986.
14. Czołczyński, K., Stateczność i drgania samowzbudne wirnika podpartego w łożyskach gazowych (Stability and self-excited vibrations of a rotor supported in gas bearings) (in Polish). *Zeszyty Nauk. Politech. Łódz. Mat.*, 1994, **694,** 2–132.
15. Czołczyński, K. and Marynowski, K., Stability of rotors supported in flexibly mounted, self-acting gas journal bearings. In *Proceedings of Ninth World Congress on the Theory of Machines and Mechanisms*, Vol 2. Milan, 1995, pp. 1199–1203.
16. Czołczyński, K. and Marynowski, K., Stability of unsymmetrical rotor supported in gas journal bearings. *Machine Vibration*, 1996, **5,** 8–17.
17. Czołczyński, K. and Marynowski, K., Stability of symmetrical rotor supported in flexibly mounted, self-acting gas journal bearings. *Wear*, 1996, **194,** 190–197.
18. Czołczyński, K. and Marynowski, K., How to avoid self-excited vibrations in symmetrical rotors supported in gas journal bearings. *Machine Dynamics Problems*, 1996, **15,** 7–20.

APPENDIX

The dimensionless parameters which are used in the main text are related to the bearing parameters and connected to their dimensional values (*) by the following formulas:

$$C_{ij}^{*}[\mathrm{N\,s/m}] = \frac{2\Lambda p_a R^2}{\omega c} C_{ij},\quad K_{ij}^{*}[\mathrm{N/m}] = \frac{p_a R^2}{c} K_{ij},\quad m^{*}[\mathrm{kg}] = \frac{4\Lambda^2 p_a R^2}{\omega^2 c} m,\quad B^{*}[\mathrm{kg\,m^2}] = \frac{4\Lambda^2 p_a R^4}{\omega^2 c} B,$$

$$\omega[\mathrm{rad/s}] = \frac{p_a c^2}{6\sigma R^2}\Lambda,\quad \nu^{*}[\mathrm{rad/s}] = \frac{\omega}{2\Lambda}\nu,\quad t[\mathrm{s}] = \frac{2\Lambda}{\omega}\tau,\quad l^{*}[\mathrm{m}] = Rl,\quad F^{*} = \frac{1}{p_a R^2} F.$$